

Modulating the magnetosphere of magnetars by internal magneto-elastic oscillations

Michael Gabler^{1,2}, Pablo Cerdá-Durán², Nikolaos Stergioulas³, José A. Font²,
and Ewald Müller¹

¹Max-Planck-Institut für Astrophysik, Karl-Schwarzschild-Str. 1, D-85741 Garching, Germany

²Departamento de Astronomía y Astrofísica, Universitat de València, 46100 Burjassot (Valencia), Spain

³Department of Physics, Aristotle University of Thessaloniki, Thessaloniki 54124, Greece

2 October 2018

ABSTRACT

We couple internal torsional, magneto-elastic oscillations of highly magnetized neutron stars (magnetars) to their magnetospheres. The corresponding axisymmetric perturbations of the external magnetic field configuration evolve as a sequence of linear, force-free equilibria that are completely determined by the background magnetic field configuration and by the perturbations of the magnetic field at the surface. The perturbations are obtained from simulations of magneto-elastic oscillations in the interior of the magnetar. While such oscillations can excite travelling Alfvén waves in the exterior of the star only in a very limited region close to the poles, they still modulate the near magnetosphere by inducing a time-dependent twist between the foot-points of closed magnetic field lines that exit the star at a polar angle $\gtrsim 0.19$ rad. Moreover, we find that for a dipole-like background magnetic field configuration the magnetic field modulations in the magnetosphere, driven by internal oscillations, can only be symmetric with respect to the equator. This is in agreement with our previous findings, where we interpreted the observed quasi-periodic oscillations in the X-ray tail of magnetar bursts as driven by the family of internal magneto-elastic oscillations with symmetric magnetic field perturbations.

Key words: asteroseismology - MHD - stars: magnetars - stars: neutron - stars: oscillations.

1 INTRODUCTION

Magneto-elastic oscillations of highly magnetized neutron stars (magnetars) may allow for the first time to infer the interior properties of these compact objects. Several groups have investigated their torsional magneto-elastic oscillations (or Alfvén oscillations when the crust is neglected) (see Levin 2007; Sotani et al. 2008; Cerdá-Durán et al. 2009; Colaiuda et al. 2009; Colaiuda & Kokkotas 2011, 2012; van Hoven & Levin 2011, 2012; Gabler et al. 2011, 2012, 2013a, and references therein). The latest models even include effects of superfluid neutrons in the core of the magnetar (Gabler et al. 2013b; Passamonti & Lander 2014). Most interestingly, the modulation of the external magnetosphere by these internal oscillations may have been detected as quasi-periodic oscillations (QPOs) in the aftermath of two out of the three observed giant flares of magnetars. In 2004, the soft gamma-ray repeater SGR 1806-20 showed the following QPO frequencies in the decaying tail of its giant flare: 18, 26, 30, 92, 150, 625, and 1840 Hz. Oscillation frequencies have also been found in the 1998 giant flare of SGR 1900+14 at 28, 53, 84, and 155 Hz. A strong motivation for linking internal magneto-elastic oscillations with the observed QPOs is the fact that several of the observed frequencies appear in a 1:3:5 ratio (as pointed out in Sotani et al. 2008), which cannot be easily ob-

tained in models that rely on predominantly crustal oscillations, but which is obtained naturally in the simplest magneto-elastic model with a purely dipole magnetic field and a regular fluid.

If the magneto-elastic oscillations can explain the observed QPO frequencies, the open question is: how can these internal oscillations modulate the emission process in the magnetosphere? A promising mechanism is the *resonant cyclotron scattering* (RCS) of photons in the magnetosphere (Timokhin et al. 2008). The fundamental ingredients for the RCS are the magnetic field configuration, the seed spectrum of the photons and the scattering targets for photons. In the magnetosphere the targets are given by the electric currents that are induced by a twist in the external magnetic field (Thompson et al. 2002).

In previous work on the RCS (Fernández & Thompson 2007; Nobili et al. 2008; Rea et al. 2008; Zane et al. 2009) the magnetic field was assumed to have a self-similar solution with possibly multipolar components (Pavan et al. 2009). More complicated magnetic field geometries have been studied in Viganò et al. (2011) and Parfrey et al. (2013). Beloborodov (2009) showed that a twisted magnetic field becomes untwisted by Ohmic dissipation of the magnetic energy. In none of these studies the magnetic field has been obtained consistently with an interior solution.

First equilibrium solutions of coupled interior and exterior fields with non-vanishing toroidal fields have been recently obtained in Glampedakis et al. (2014). However, these equilibria have not been used for calculations of RCS and, because they are equilibrium solutions with particular current configurations they cannot be used for dynamical simulations. To study the interior and exterior magnetic field evolution of neutron stars in a consistent framework different groups have developed numerical tools that are based either on resistive magneto hydrodynamics (MHD) or on some matching between ideal MHD to its force-free limit (Bucciantini & Del Zanna 2013; Dionysopoulou et al. 2013; Palenzuela 2013; Paschalidis & Shapiro 2013).

First studies of the coupling of the magnetosphere to internal oscillations of magnetars have been recently reported in Link (2014) and Kojima & Kato (2014). The latter use a model of resistive electrodynamics with artificially low conductivity of the plasma that is not expected around magnetars (Thompson et al. 2002; Beloborodov & Thompson 2007; Beloborodov 2009, 2013a). An appropriate description of the magnetosphere of magnetars has to be in terms of the force-free approximation that we adopt here.

The aim of this paper is to couple the internal magneto-elastic oscillations of magnetars to their exterior magnetospheres. We construct linear, force-free magnetic field configurations that are completely determined by the background configuration and by torsional perturbations of the magnetic field at the surface, which are obtained by numerical simulations as in Cerdá-Durán et al. (2009) and Gabler et al. (2011, 2012, 2013a,b). These configurations are compared to twisted, self-similar configurations with dipolar background fields (Thompson et al. 2002) to check the validity of our approach. In our model, the internal oscillations can couple to the exterior through the closed magnetic field lines and produce time modulations of the magnetosphere. This is in contrast to Link (2014), who finds that the transmission of Alfvén waves from the neutron star crust to the magnetosphere is strongly suppressed due to the strong impedance mismatch between the two regions. In this work, we show that this hampered transmission is only relevant for a small region of open magnetic field lines near the rotational axis.

The paper is organized as follows: in Section 2, we discuss how we construct force-free equilibria magnetic field configurations in the neutron star exterior by prescribing the axisymmetric magnetic field perturbation at the surface. The corresponding results are given in Section 3. In Section 4, we discuss how the interior oscillations change the exterior magnetic field in the absence of Alfvén waves. Finally, a summary is provided in Section 5.

2 MAGNETIC FIELD CONFIGURATION

The time-scale of magneto-elastic oscillations with frequency $f \lesssim 150$ Hz inside a magnetar is of the order of $t_{\text{QPO}} \gtrsim 0.007$ s (Gabler et al. 2012, 2013a,b). In the magnetosphere, the Alfvén speed is approximately equal to the speed of light and thus, out to a distance of $r \lesssim 1000$ km, the dynamical time-scale is, $t_{\text{mag}} \sim r/c \sim 1/300$ s $< t_{\text{QPO}}$. In the near magnetosphere, where closed field lines close within a distance of tens up to a few hundreds of km, $t_{\text{mag}} \ll t_{\text{QPO}}$. Therefore, we assume that the reconfiguration of the external field occurs on a much shorter dynamical time-scale than the period of the low-frequency, internal magneto-elastic oscillations (our argument does not apply to the high-frequency QPOs, which would require separate considerations). By treating this fast relaxation as if it effectively occurred instantaneously, the exterior magnetic field reaches an equilibrium configuration that is deter-

mined by the surface magnetic field. We thus construct a sequence of static equilibria in the magnetosphere, and model the modulation of the magnetosphere by internal oscillations as a quasi-static evolution. Typical rotation periods of magnetars $P \sim 10$ s are much longer than the QPO time-scale and we thus neglect rotational effects.

The magnetic field in the magnetosphere can be assumed to be force-free. In this approximation, the inertia and momenta of the charge carriers are neglected with respect to the magnetic field energy density ($\{\rho, p\} \ll B^2$), where ρ is the density, p is the pressure and B is the magnetic field strength. Consequently, the momentum equation leads to the force-free condition

$$\mathbf{J} \times \mathbf{B} = 0, \quad (1)$$

where \mathbf{J} is the current density. This equation states that the currents have to flow along magnetic field lines, and, hence, that in equilibrium no Lorentz force is acting on the charge carriers.

Such a configuration can be maintained only under the assumption of ideal MHD. In particular, this means that there have to be sufficiently many charge carriers to make the medium (practically) perfectly conducting. In the quiescent state of SGRs, the charge carriers are provided by a strong and twisted magnetic field. Its toroidal component B_φ creates a large difference in the electric potential between the foot-points of the field lines that are anchored in the crust. This potential is sufficiently strong to accelerate electrons and light ions from the atmosphere just above the surface of the neutron star (formed by thermally excited particles) along the magnetic field lines (Thompson et al. 2000). The number of these charge carriers is by far not sufficient to create the required currents. However, particles that are accelerated along the magnetic field lines create e^+e^- pairs when reaching the energy threshold for this process. This condition is easily fulfilled in the case of magnetars. In turn, the pairs get accelerated in the direction of opposite potential and can create further pairs when having acquired sufficient kinetic energy. Finally, these pair avalanches fill the magnetosphere with sufficient plasma to conduct the current (Beloborodov & Thompson 2007; Beloborodov 2013a,b). How this scenario is changed in the case of a giant flare is not clear and needs further investigation. Here, we assume that the modulation due to the internal oscillations occurs on field lines that extend to slightly larger radii $r \gtrsim 20$ km than those field lines that are expected to host the fireball of the giant flare.

Any static twist of the magnetic field will dissipate on the time-scale of years (Beloborodov & Thompson 2007; Beloborodov 2009). This is orders of magnitude longer than the time-scale of interest for giant flares (~ 400 s) and of their QPOs ($\lesssim 4$ min), i.e. we can safely neglect dissipation in the magnetosphere, and the assumption of ideal MHD holds.

2.1 Self-similar fields

One solution of equation (1) is given by currents along the magnetic field $\mathbf{J} = \nabla \times \mathbf{B} = \mathcal{P}(\Gamma)\mathbf{B}$, where \mathcal{P} is a proportionality factor and Γ is a flux parameter (see Thompson et al. 2002, for details). By making a particular ansatz for Γ one arrives at a *self-similar solution*, i.e. all magnetic field components decay with the same power law

$$B_i \sim r^{-2-q}, \quad (2)$$

where q is an index. The corresponding configuration can be described by the global twist $\Delta\Phi$ that is defined as the twist angle

between the foot-points of a closed field line that is anchored near the poles ($\theta \rightarrow 0$)

$$\Delta\Phi = 2 \int_{\theta}^{\pi/2} \frac{B_{\varphi}(\theta)}{B_{\theta}(\theta) \sin \theta} d\theta. \quad (3)$$

In the self-similar model, the choice of Γ and of the parameter $\Delta\Phi$ completely defines the current distribution. However, only very particular global twisted magnetic fields can be prescribed. For small values of $\Delta\Phi \lesssim 0.1$ the configuration remains very similar to a pure dipole configuration, with $q \sim 1.0$.

2.2 Force-free magnetic fields in the Schwarzschild spacetime

The mass of a neutron star causes a significant curvature of the spacetime and hence also affects the structure of the magnetic field. For this reason, the internal magneto-elastic oscillations are computed with a general-relativistic code. To describe the magnetosphere consistently and to match it to our interior configurations (Gabler et al. 2012, 2013a,b), we thus consider a general-relativistic metric using units with $G = c = 1$. In the exterior, we can assume the metric of a spherically symmetric star, i.e. the Schwarzschild metric

$$ds^2 = -\alpha^2 dt^2 + \alpha^{-2} dr^2 + r^2 (d\theta^2 + \sin^2 \theta d\varphi^2), \quad (4)$$

where $\alpha \equiv (1 - 2M/r)^{1/2}$ is the lapse, and M is the mass of the star. Compared to a Newtonian configuration of the same mass, the difference in the magnetic field structure near the stellar surface is of the order of several percent.

We follow Uzdensky (2004) and use an orthonormal basis $e_k = \gamma_{kk}^{-1/2} \partial_k$ with $k = \{r, \theta, \varphi\}$ and γ_{ij} being the 3-metric in the usual 3 + 1 split of the spacetime. Correspondingly, the 3-dimensional vector operators are ∇f (the gradient), $\nabla \cdot \mathbf{B}$ (the divergence), and $\nabla \times \mathbf{B}$ (the curl). We use a tilde to indicate vector components that are given in the usual co- or contravariant basis as $V_k = \gamma_{kk}^{-1/2} V_{\tilde{k}} = \gamma_{kk}^{1/2} V^{\tilde{k}}$. The relevant Maxwell equations take the following form in the 3 + 1 split of the Schwarzschild geometry (MacDonald & Thorne 1982; Uzdensky 2004)

$$\nabla \cdot \mathbf{B} = 0 \quad (5)$$

$$\nabla \times (\alpha \mathbf{B}) = \alpha \mathbf{J}. \quad (6)$$

In this formulation, the Newtonian limit is recovered by setting $\alpha = 1$.

2.3 Linear reconstruction of δB_{φ} as a flux function

For an equilibrium background configuration condition (1) has to be fulfilled. Considering axisymmetric perturbations up to linear order, the poloidal components of equation (1) remain unchanged, while the φ -component has to satisfy the condition

$$\begin{aligned} 0 &= (\mathbf{J} \times \mathbf{B})_{\varphi} \\ &= \frac{1}{r} \left[\frac{B_{\theta}}{\sin \theta} (\sin \theta \delta B_{\varphi})_{,\theta} + B_r (r \alpha \delta B_{\varphi})_{,r} \right] \\ &= \frac{1}{\alpha r \sin \theta} (\mathbf{B}_0 \cdot \nabla) (\alpha r \sin \theta \delta B_{\varphi}), \end{aligned} \quad (7)$$

where \mathbf{B}_0 is the poloidal background field, δB_{φ} is the magnetic field perturbation in the φ direction, and a comma denotes a partial derivative. equation (7) states that $\alpha r \sin \theta \delta B_{\varphi}$ does not change in the direction of the background field, i.e. this term is a flux function that is constant along field lines.

The magnetic vector potential $A_{\tilde{\varphi}} = \gamma_{\varphi\varphi}^{1/2} A_{\varphi} = r \sin \theta A_{\varphi}$ is also a flux function whose equipotential lines coincide with the field lines. The φ -component of $0 = \mathbf{B} \times \mathbf{B}$ together with the definitions $B_{\theta} = -F_{\varphi r}$, $B_r = F_{\varphi\theta}$, and $F_{\tilde{\mu}\tilde{\nu}} = A_{\tilde{\mu},\tilde{\nu}} - A_{\tilde{\nu},\tilde{\mu}}$ give $\mathbf{B} \cdot \nabla A_{\tilde{\varphi}} = 0$, i.e. the gradient of $A_{\tilde{\varphi}}$ is perpendicular to the magnetic field direction. Hence, $A_{\tilde{\varphi}}$ is constant in the direction of \mathbf{B} , and we can use $A_{\tilde{\varphi}}$ to extend δB_{φ} from the magnetar surface into the magnetosphere.

In practice, we consider the value of the potential $A_{\tilde{\varphi}}$ at some location \mathbf{r}_x in the magnetosphere and find the corresponding magnetic field perturbation δB_{φ} at the surface location \mathbf{r}_s , which has the same value of $A_{\tilde{\varphi}}$ by using a 4-point Lagrange interpolation. In this way, we construct

$$\delta B(\mathbf{r}) = \frac{\alpha_s r_s \sin \theta_s}{\alpha_x r_x \sin \theta_x} \delta B_{\varphi}(\mathbf{r}_s). \quad (8)$$

This approach based on linear reconstruction is very efficient, because it provides an explicit expression of the φ -component of the magnetic field in the magnetosphere, if the background poloidal field \mathbf{B}_0 or its potential $A_{\tilde{\varphi}}$ is given. Moreover, we can directly construct the field in the magnetosphere from the magnetic field at the magnetar surface. As the background configuration is known to larger radii than the numerical domain we consider here, no further boundary conditions need to be specified at the outer boundary of the numerical grid.

In this work we restrict ourselves to magnetic field configurations with $\delta B_{\varphi}/B_0 \lesssim 0.1$, for which the linear approximation is valid. Thus, we can safely neglect corrections of the poloidal magnetic field by the twist induced by torsional oscillations.

We obtain the magnetar's surface magnetic field from our simulations of magneto-elastic oscillations in the magnetar interior (Gabler et al. 2012, 2013a) using background magnetic fields computed either with the MAGNETSTAR (Gabler et al. 2013a) routine of the LORENE¹ library or with an extension of the RNS code (Stergioulas & Friedman 1995; Friedman & Stergioulas 2013). The background model also provides the poloidal magnetic field in the magnetosphere.

2.4 Analytic solution in the Newtonian approximation

In a Newtonian framework, we can derive an analytic solution of the linearized twisted dipole and compare it to the self-similar solution. For a background dipole (poloidal) field $B_r = 2m_B \cos \theta / r^3$ and $B_{\theta} = m_B \sin \theta / r^3$, where m_B is a measure of the magnitude of the magnetic field, and by using equation (7) with $\alpha = 1$, we obtain

$$\begin{aligned} 0 &= \frac{1}{r^3} \left[2m_B \cos \theta (r \delta B_{\varphi})_{,r} + \frac{m_B}{r} (r \sin \theta \delta B_{\varphi})_{,\theta} \right] \\ &= 2 \cos \theta (r \delta B_{\varphi})_{,r} + (\sin \theta \delta B_{\varphi})_{,\theta}. \end{aligned} \quad (9)$$

Separating variables as $\delta B_{\varphi} \equiv f(\theta)g(r)$ gives

$$2 \frac{[rg(r)]_{,r}}{g(r)} = - \frac{[\sin \theta f(\theta)]_{,\sin \theta}}{f(\theta)}. \quad (10)$$

With the corresponding solution $g(r) \equiv r^{\kappa}$ and $f(\theta) \equiv \sin^{\lambda} \theta$ we obtain the relation

$$\kappa = - \frac{\lambda + 3}{2}, \quad (11)$$

and thus

¹ <http://www.lorene.obspm.fr>

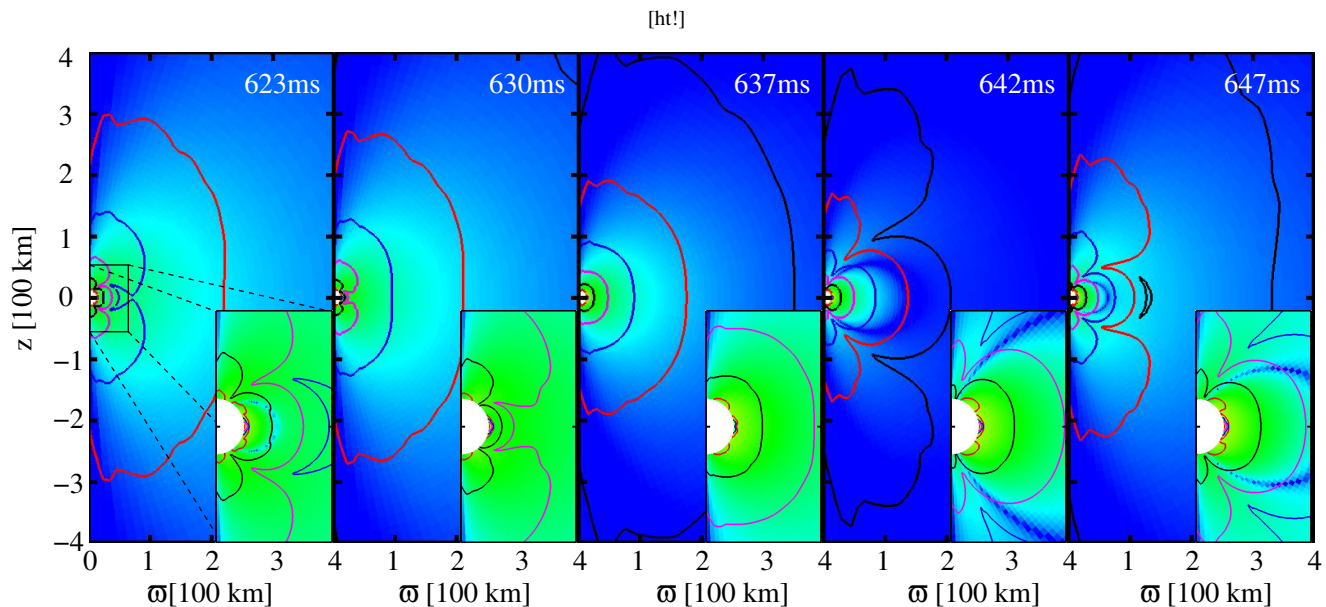


Figure 1. Snapshots of the quasi-static evolution of the logarithm of the toroidal magnetic field perturbation δB_φ in the magnetosphere, matched to an interior simulation of magneto-elastic oscillations. The background poloidal magnetic field strength is $B = 3 \times 10^{15}$ G, while the toroidal one is $\sim 10^{14}$ G. The colour scale is the same in all panels and ranges from blue (10^8 G) to orange-red (10^{14} G). The solid lines correspond to constant current surfaces of the absolute value of the poloidal current. The snapshot time is given in the top-right corner of each panel. The inset in the bottom-right corner of each panel gives a magnification of the innermost 50 km.

$$\delta B_\varphi = r^{-\frac{\lambda+3}{2}} \sin^\lambda \theta. \quad (12)$$

One sees that δB_φ has a different fall-off behaviour with r than B_r , B_θ , in contrast to the self-similar solutions that correspond to the particular choice $\lambda = 3$.

3 RESULTS

In this section, we discuss the first implications of our model, that for dipole-like background magnetic fields there can be no anti-symmetric perturbations δB_φ in the magnetosphere. We then construct configurations that are matched to simulations of the interior in order to describe the evolution of the magnetic field consistently. Finally, the range of validity of the magnetic field reconstruction method is studied.

3.1 Exclusion of antisymmetric perturbations δB_φ for dipole-like background magnetic fields

In equation (7) we found that $\alpha r \sin \theta \delta B_\varphi$ is a flux function, i.e. this expression has to be constant along field lines. For dipole-like fields that connect the two hemispheres of the star and because α , r and $\sin \theta$ are all symmetric with respect to the equator, only symmetric configurations of the torsional magnetic field δB_φ can lead to force-free equilibria. This holds not only for dipole-like background fields, but also for more complicated configurations with field lines exiting and entering the star at symmetric locations with respect to the equatorial plane.

An antisymmetric perturbation δB_φ implies a symmetric torsional velocity perturbation δv_φ . In this case, both foot-points of a magnetic field line move with the same speed in the same direction, i.e. the magnetic field line does not become twisted. In a dynamic (i.e. non-perturbative) calculation the field line would bend,

because δv_φ would change along the field line. However, there exists no equilibrium solution in this general situation other than the velocity being zero, and hence $\delta B_\varphi = 0$. This in turn implies that there are no persistent currents (for $t > t_{\text{mag}}$) along the field lines and the emitted radiation will not be modulated. In contrast, for symmetric magnetic field perturbations, the twist of the magnetic field lines is maintained for $t > t_{\text{mag}}$ because the locations of their foot-points evolve on much longer time-scales ($t_{\text{QPO}} > t_{\text{mag}}$) that are defined by the magnetar's interior oscillations.

3.2 Configurations matched to the interior

The magnetic field configurations in the magnetosphere are obtained from simulations of the magneto-elastic oscillations of magnetars (Gabler et al. 2011, 2012, 2013a,b). From these simulations, we obtain (as a function of time) the magnetic field perturbation δB_φ at the surface of the magnetar for a given background poloidal magnetic field \mathbf{B}_0 in the magnetosphere. With this information, we reconstruct the magnetic field perturbation δB_φ of a force-free equilibrium in the magnetosphere from equation (7). For our study, we use an equilibrium model with $R = 12.26$ km, $M = 1.4M_\odot$ and a magnetic field strength at the pole of 3×10^{15} G. The equation of state (EOS) is APR (Akmal et al. 1998) in the core, matched to the Douchin & Haensel (2001) EOS in the crust.

Fig. 1 displays snapshots from a typical quasi-static evolution of (the logarithm of) the absolute value of δB_φ in the magnetosphere towards the end of a simulation covering $t \sim 650$ ms. The solid lines are constant current surfaces of (the absolute value of) the poloidal current consistent with the toroidal magnetic field. In the magnetosphere, the numerical grid of 100×80 ($r \times \theta$) zones covers the range $[r_s, 1200 \text{ km}] \times [0, \pi]$. The radial grid spacing increases logarithmically, while the angular grid is equidistant. In Fig. 1 we show δB_φ up to a distance $\varpi = 400$ km from the mag-

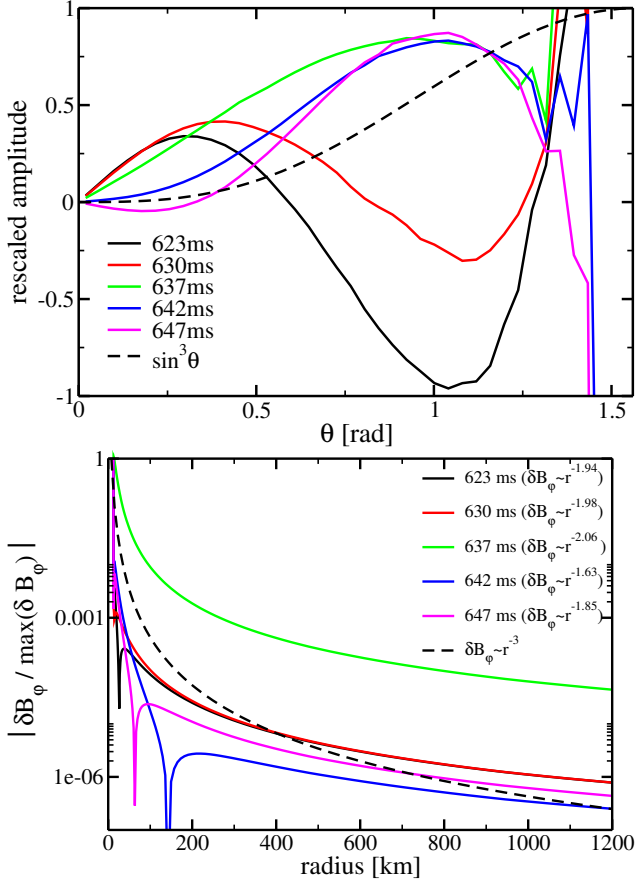


Figure 2. *Top panel:* snapshots of the magnetic field at the surface of the magnetar. The black dashed line corresponds to a self-similar solution with angular dependence $\sim \sin^3 \theta$. *Bottom panel:* Fall-off behaviour of δB_φ near the equator as a function of radius r at different times. The dashed line gives a self-similar solution with $B \sim r^{-3}$ for all components of the magnetic field. The asymptotic fall-off of B for large r is given in the upper right corner of the bottom panel.

netic field axis and up to the same distance along that axis in positive and negative direction.

At large distances, the magnetic field and the currents in our model decrease very smoothly, the latter being qualitatively similar to those of the self-similar solutions (see Section 3.3). The main differences are the stronger decrease of δB_φ with r in the self-similar case ($\lambda \sim 3$), and that for $r \lesssim 200$ km the magnetic field can be quite different from that of the self-similar solutions. As can be inferred from the nodal lines in last two panels in Fig. 1, the magnetic field can change its sign with increasing radius or with increasing polar angle. This angular dependence differs from that of the self-similar models, which possess no nodes in the θ -direction.

To investigate the magnetic field behaviour near the star, we show the angular dependence of the rescaled magnetic field at the surface in the top panel of Fig. 2 at the same times used in Fig. 1. The black dashed line in this panel is an example of a self-similar field with $\delta B_\varphi \sim \sin^3 \theta$. The figure shows that the magnetic field structure changes considerably with time. At $t = 623$ ms, δB_φ has two nodes (not counting the one at the pole), at $t = 637$ ms there are no nodes, while at $t = 647$ ms one recognizes again two nodes. In contrast, the self-similar field has no nodes. All configurations show the strongest magnetic field perturbation at the equator

Time (ms)	623	630	637	642	647
r (km)	25	15	-	150	65
θ (rad)	0.6	0.8	-	0.05	0.35

Table 1. Nodes of the magnetic field configurations in the equatorial plane (second row) and along the magnetar’s surface for $\theta < 1.0$ rad (third row) at different times.

($\theta = \pi/2$), because only symmetric perturbations δB_φ are allowed (see Section 3.1). Therefore, the velocity δv_φ and hence the displacement ξ_φ have to be antisymmetric, i.e. they both must have a node at the equator. This in turn implies that the θ -derivative of the displacement $\xi_{\varphi,\theta}$ has a maximum at the equator. The radial derivative of the displacement $\xi_{\varphi,r}$ has to be zero, because for the interior simulations we impose the continuous traction condition at the magnetar’s surface (Cerdá-Durán et al. 2009; Gabler et al. 2012). From the linearized induction equation

$$\delta B_\varphi = B_r \xi_{\varphi,r} + B_\theta \xi_{\varphi,\theta}, \quad (13)$$

one then finds that δB_φ has a maximum at the equator. In addition, B_θ has a maximum at the equator too, which gives rise to a large value of δB_φ close to the equator. The latter holds, however, only in a small region very close to the star, because the magnetic field lines of the poloidal background field originating from the region close to the equator extend only to about $\lesssim 1$ km above the surface. The remaining part of the magnetosphere remains unaffected.

The radial dependence of the magnetic field perturbation δB_φ at the equator is shown in the bottom panel of Fig. 2 at the same times as in Fig. 1. The dashed black line gives a self-similar solution that decreases as $\sim r^{-3}$, while the solid lines are solutions obtained at different times from a given magneto-elastic simulation. At small radii, δB_φ decreases for most configurations more rapidly with increasing radius than the self-similar solution. Only for the configuration at $t = 637$ ms the decrease is less rapid. For large radii $r \gtrsim 200$ km, the magnetic field perturbation δB_φ decreases in all our configurations much slower than the self-similar solution. The corresponding radial dependences are given in the upper right corner of the bottom panel of Fig. 2. They all differ significantly from r^{-3} .

The radial behaviour of δB_φ at the equator ($\theta = \pi/2$) reflects its angular behaviour at the magnetar’s surface, because both are linked via the poloidal field lines. The expression $\alpha r \sin \theta \delta B_\varphi$ has to be constant on these lines, i.e. the strong decrease at small r (see bottom panel of Fig. 2) is related to the strong decrease of δB_φ at large θ (see top panel). The nodes of the lines for $\theta < 1.0$ rad in the top panel correspond to the nodes for $r < 200$ km in the bottom one. The corresponding values of r and θ , where the magnetic field possesses nodes, are given in Table 1. Besides the strong decrease at large angles all fields, but the one at 637 ms (green line), show a node at about $\theta \gtrsim 1.3$ rad (see top panel of Fig. 2). The corresponding node in radial direction is located only a few kilometers above the surface, i.e. it cannot be recognized in the bottom panel.

The fall-off behaviour of δB_φ at large radii is determined by its decrease on the magnetar’s surface very close to the pole. The steeper the gradient of δB_φ is as a function of θ at the surface, the stronger is the decrease at large r . The steepest fall-offs are obtained at $t = 637$, 630, and 623 ms, respectively (see bottom panel of Fig. 2).

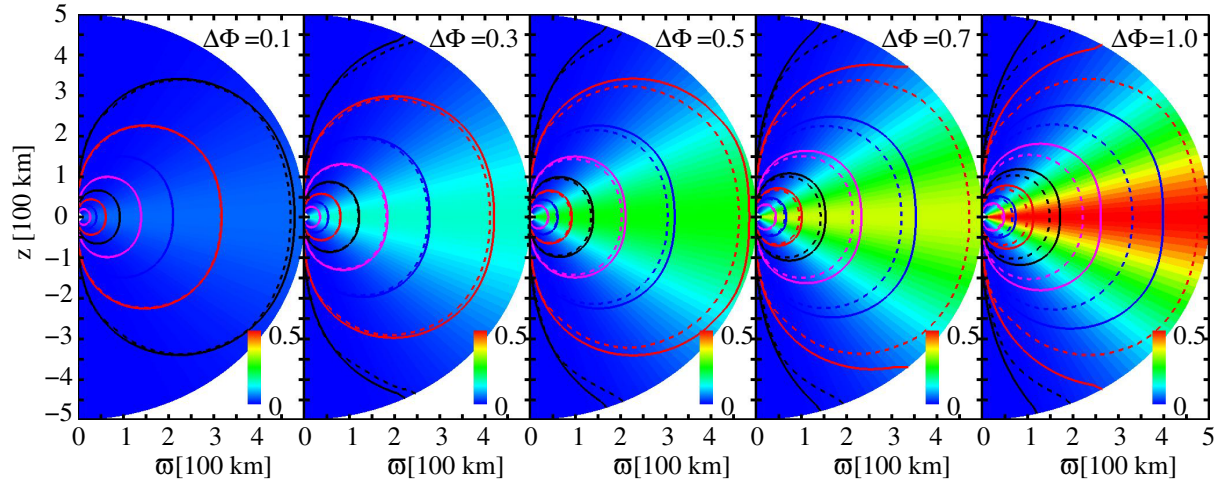


Figure 3. Ratio of $\delta B_\varphi/B_0$ in the magnetosphere for *self-similar* magnetic field configurations (colour coded), the solid lines showing constant current surfaces. In comparison, the dashed lines show constant current surfaces obtained with the *linear reconstruction method*, where the magnetic field at the magnetar’s surface was chosen to agree with that of the self-similar solution. The value for $\Delta\Phi$ given in the different panels denotes the total twist and hence a measure of the strength of the toroidal magnetic field component relative to the background poloidal component (see equation 3).

3.3 Range of validity of linear models

To construct our models, we assume a linear perturbation in δB_φ . In contrast the self-similar solutions are nonlinear, i.e. they can be used to check the validity of our approximation. In Fig. 3 we show the ratio of toroidal and poloidal magnetic field strength, $\delta B_\varphi/B_0$, for different self-similar solutions with twist angles $\Delta\Phi = \{0.1, 0.3, 0.5, 0.7, 1.0\}$. With increasing $\Delta\Phi$, the relative strength of the toroidal field component increases and reaches the same order of magnitude as the poloidal one at the equator, for $\Delta\Phi = 1.0$. In a nonlinear treatment, such a strong toroidal magnetic field would lead to an inflation of the poloidal component (Roumeliotis et al. 1994; Viganò et al. 2011).

The solid lines in Fig. 3 represent constant poloidal current surfaces that is consistent with the toroidal magnetic field component of a self-similar solution, while the dashed lines are obtained with our linear reconstruction method. The same colours representing the same current magnitudes. For a weak twist ($\Delta\Phi = 0.1$, first panel) the lines for the self-similar and linear method are almost indistinguishable, i.e. both methods give approximately the same currents. The stronger the twist, the more the linear results differ from the self-similar ones. For the strongest twist shown in the last panel ($\Delta\Phi = 1.0$) the constant poloidal current surfaces differ significantly among the two approaches. In the linear case we underestimate the currents, because we neglect the toroidal currents that are present in the nonlinear, self-similar configurations. Additionally, the poloidal magnetic field inflates in the latter case, i.e. the poloidal currents extend further into the magnetosphere. Therefore, the blue dashed line (linear method) crosses the equator closer to the star at ~ 330 km than the solid line (self-similar solution) that crosses at ~ 400 km. Despite these quantitative differences, the general shape of the constant current surfaces is very similar for both the linear approximation and the self-similar solution.

Based on the differences in the currents, the configuration with $\Delta\Phi = 0.5$ can be regarded as the limiting case up to which one can apply the linear reconstruction method. For this configuration the ratio of the toroidal and poloidal magnetic field strength is less than 25% and the current amplitudes at $r = 100$ km of the reconstructed field and the self-similar solution differ by less than 5%.

Time (ms)	623	630	637	642	647
$\delta B_\varphi/B_0$	0.08	0.06	0.02	0.03	0.06

Table 2. Maximum values of $\delta B_\varphi/B_0$ for the five quasi-stationary configurations considered in our study. The maxima are always located at the outer boundary of the computational domain at $r \sim 1200$ km and $\theta = \pi/2$.

In our models we employed a *more conservative estimate* of the maximum acceptable toroidal magnetic field and assumed the linear approximation to be valid up to $\delta B_\varphi/B_0 \leq 0.1$.

We give the maximum of $\delta B_\varphi/B_0$ for the five magnetic field configurations displayed in Fig. 1 in Table 2. It never exceeds a value of 0.1 in the computational domain that extends up to $r = 1200$ km, and is always located at the most distant points of the computational grid in the equatorial plane. This is a consequence of the fact that the fall-off of the toroidal magnetic field perturbation $\delta B_\varphi \sim r^{-1.5 \dots -2.1}$ is less steep than that of the poloidal background field $B \sim r^{-3}$. The linear reconstruction method is thus a very good approximation up to distances of $r \sim 1000$ km.

4 TRANSMISSION OF ALFVÉN WAVES

In a recent paper, Link (2014) studied the transmission of torsional Alfvén waves from the magnetar’s interior into its magnetosphere. He found that most of the energy of the oscillations cannot be transmitted, because of the very different propagation speeds in the two regions. However, this conclusion only holds in his plane-parallel toy model, where waves can be excited in the exterior along open magnetic field lines. As we show next, *when a more realistic model of a global dipolar magnetic field is considered, the considerations of Link (2014) are relevant only for field lines very close to the magnetic poles.*

To allow for torsional Alfvén wave transmission along magnetic field lines, the lengths of the field lines l_{fl} have to be larger than the wavelength λ_f of an oscillation at given frequency f . At $f \sim 150$ Hz the corresponding wavelength is $\lambda_f \sim \frac{c}{f} \gtrsim 2000$ km. Assuming a dipole-like background magnetic field configuration,

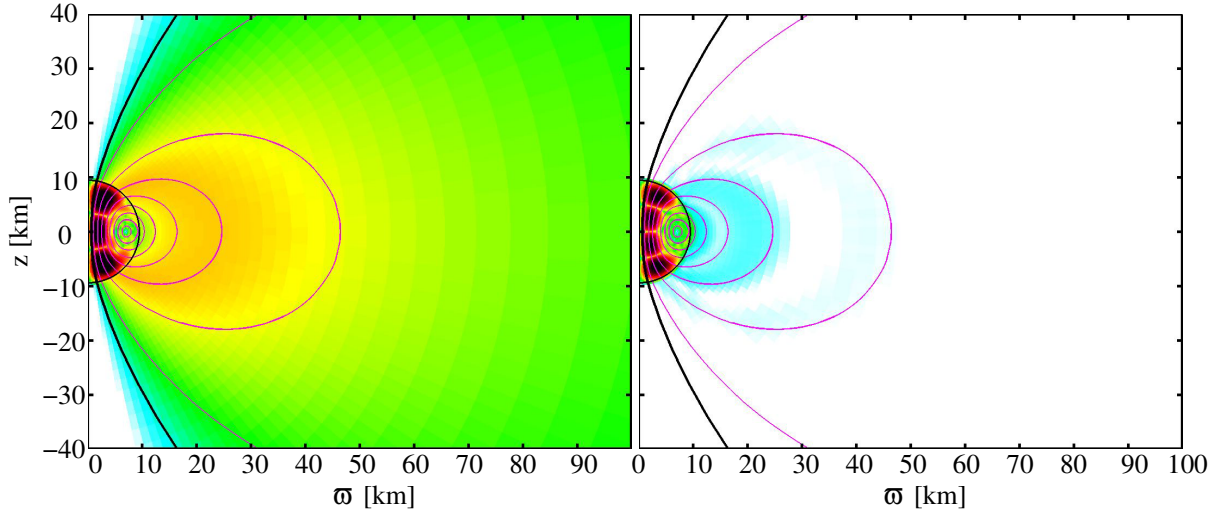


Figure 4. Rescaled absolute value of the Fourier amplitude of the evolution of the toroidal magnetic field perturbation δB^φ for a perturbation with a frequency of $f = 22$ Hz that is symmetric (left-hand panel) and with a frequency of $f = 29$ Hz that is antisymmetric (right-hand panel) with respect to the equator. The solid lines show magnetic field lines. To the right of the solid thick black line is the region where Alfvén waves with $f < 150$ Hz cannot propagate. The logarithmic colour scale ranges from white-turquoise (10^{-7}), green (10^{-4}), yellow (10^{-3}) to red-black (1). The perturbation of the exterior magnetic field is orders of magnitude smaller in case of an antisymmetric perturbation inside the star (right-hand panel) than in case of a symmetric one (left-hand panel).

the corresponding limiting field line has a maximum extent of approximately $\varpi \sim 300$ km, and intersects the magnetar’s surface approximately at $\theta \sim 0.19$ rad. Thus, Alfvén wave transmission can take place only at very small polar angles, i.e. in a narrow cone along the axis of the magnetic field. Our estimate $\theta \lesssim 0.19$ rad is rather conservative, because even for $l_{\text{fl}} > \lambda_f$ the waves cannot travel freely along magnetic field lines. Closed magnetic field lines that are anchored to the crust can only be excited to oscillate at certain frequencies. The latter depend on the length of the field line, the magnetic field strength, and the boundary condition imposed at the stellar surface. For a complete description one would have to solve the coupled core-crust-magnetosphere problem which is computationally expensive. However, for the frequencies of interest here, $f \lesssim 150$ Hz, and thus for field lines exiting the star at $\theta \gtrsim 0.19$ rad, we can apply the approximations described above.

We confirmed the correctness of our argumentation by performing a simulation (extending up to $t = 1$ s) of internal Alfvén oscillations with the GRMHD code MCOCOA (Cerdá-Durán et al. 2008, 2009; Gabler et al. 2012). The simulation setup includes a very low density, artificial atmosphere which extends up to $r \lesssim 1000$ km. The density at the surface is set to $\rho_s = 10^{-10} \rho_{\text{center}} \sim 4 \times 10^5 \text{ g cm}^{-3}$. To guarantee an approximately constant Alfvén velocity $v_A \sim c$ in the atmosphere, the density falls off as r^{-4} . For the simulation, we use our fiducial equilibrium model with a dipole field strength of $B = 10^{15}$ G and neglect the crust. In the outer parts of the crust, magnetic forces are much stronger than shear forces, i.e. the magnetic field dominates the coupling to the exterior. Therefore, the influence of the crust can be safely neglected even though its presence could affect the structure of particular internal oscillations and could also shift their frequencies by some small amount. The initial perturbation of the equilibrium configuration has a mixed $l = 2$ and $l = 3$ angular dependence. At the surface of the magnetar we need not to prescribe boundary conditions, because the continuous traction condition used by Cerdá-Durán et al. (2009) and Gabler et al. (2012) is equivalent to momentum conservation which is guaranteed by our numerical MHD scheme. At the

outer boundary, we explicitly apply the continuous traction condition which does not allow for surface currents (see Cerdá-Durán et al. 2009; Gabler et al. 2012, for details).

Fig. 4 shows the (absolute value of the) Fourier amplitude of the toroidal magnetic field component δB^φ that is created in the magnetosphere by the coupling to an internal Alfvén oscillation. The left-hand panel shows the amplitude corresponding to a particular oscillation with a frequency of 22 Hz that is symmetric (in δB^φ) with respect to the equatorial plane, while the right-hand panel displays an antisymmetric oscillation at $f = 29$ Hz. Note that in our previous work (e.g. Cerdá-Durán et al. 2009; Gabler et al. 2011, 2013a) we used the velocity to compute the Fourier amplitude, and that the velocity has always a maximum where the magnetic field has a node and vice versa. Travelling Alfvén waves with $f \lesssim 150$ Hz can be transmitted only in the region to the left of the thick black magnetic field line in the figure, where the wavelength $\lambda_{150 \text{ Hz}} < l_{\text{fl}}$.

In the near magnetosphere ($r \lesssim 100$ km), the external field relaxes almost instantaneously (compared to the interior evolution time-scale) to a force-free equilibrium, whose configuration is determined by the structure and the amplitude of the perturbation at the magnetar’s surface (see previous sections). The resulting magnetic field structure does not resemble one that could be produced by standing Alfvén waves. The latter would give rise to nodes along the field line, whereas each configuration considered here has a static twist $\delta B^\varphi \neq 0$ everywhere along a given field line, i.e. there are no nodes. From equation (7), we expect $\alpha \delta B^\varphi = \alpha r \sin \theta \delta B_\varphi$ to be constant along magnetic field lines. Although the interior oscillations of the magnetar shown in the two panels of Fig. 4 have different symmetries, we find that the condition $\delta B^\varphi = \text{const.}$ holds approximately in both cases. Small deviations at small radii are caused by the factor α whose influence we do not consider in this figure.

Fig. 4 also shows that for antisymmetric interior oscillations (right-hand panel) the amplitude of the exterior magnetic field perturbation is orders of magnitudes smaller (white and turquoise re-

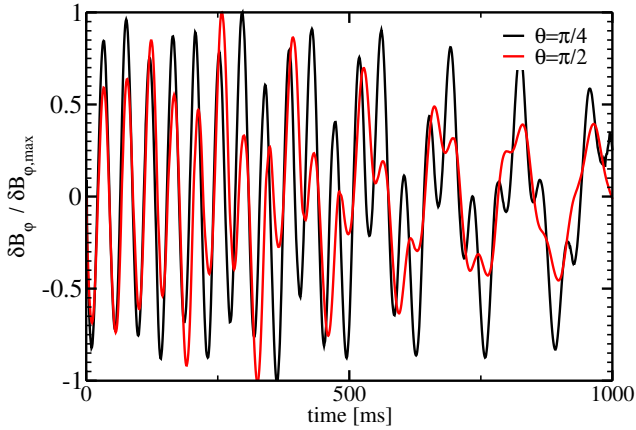


Figure 5. Time evolution of δB_ϕ at $r = 51$ km and two polar angles θ rescaled to its maximum value.

gions) than for symmetric oscillations (left-hand panel). In addition, we note that outside the star δB_ϕ is symmetric with respect to the equator, too². Our simulations confirm the result of our linear reconstruction method that antisymmetric oscillations cannot be communicated to the exterior in the near magnetosphere.

In Fig. 5, we illustrate the evolution of the magnetic field perturbation δB_ϕ at $r = 51$ km and $\theta = \pi/2$ and $\theta = \pi/4$, respectively. The exterior field is clearly modulated at the frequencies that are determined by the interior oscillations.

The study presented in this section shows that the amplitude of the modulations of the near magnetosphere caused by internal oscillations is not limited by the reflection of plane-parallel waves as calculated by Link (2014). Instead, the amplitude of the modulations is determined by how much the exterior field is twisted by the motion of the foot-points of the magnetic field lines that are anchored to the crust. These quasi-static modulations of the magnetospheric field can lead to modulations in the X-ray emission and thus may cause the observed QPOs, through e.g. the resonant cyclotron scattering process.

5 CONCLUSIONS

In this paper we have investigated how the low frequency ($f \lesssim 150$ Hz) torsional magneto-elastic oscillations of a magnetar can modulate the exterior magnetic field. In addition, we have shown that these oscillations are relevant for Alfvén wave transmission only along field lines that arise within a very narrow cone ($\theta \lesssim 0.19$ rad) around the polar axis. Here, we are mainly interested in what happens during a giant flare that is supposed to produce a fireball close to the magnetar’s surface (Thompson & Duncan 2001). In this region, the magnetospheric field finds its force-free equilibrium configuration much faster than the internal oscillation time-scale, i.e. the magnetosphere evolves quasi-statically through a sequence of force-free equilibria. However, at any given time the internal oscillations determine the magnetic field at the magnetar’s surface. The shift of the foot-points of the external magnetic field lines relative to the unperturbed configuration twists the external magnetic

² This is an artefact of the FFT which has a limited resolution in the frequency domain, resulting in an overlap of oscillations at frequencies very close to a given frequency.

field, i.e. the field is no longer a potential field and currents flow in the magnetosphere.

For a dipole background magnetic field we have shown that only axisymmetric, torsional magnetic field perturbations that are symmetric with respect to the equator are allowed (the corresponding velocity perturbation is antisymmetric). That only symmetric perturbations are viable is a promising result, because the frequencies of the low-frequency QPOs observed in the two giant flare sources come in a near 1 : 3 : 5 ratio, as pointed out first by Sotani et al. (2008) who, however, studied only purely Alfvén oscillations. For the case of global magneto-elastic oscillations we found (Cerdá-Durán et al. 2009; Gabler et al. 2012) that for sufficiently strong dipole magnetic fields (when the oscillations can penetrate the crust and reach the surface) symmetric oscillations of δB_ϕ also have approximately the same odd-integer 1 : 3 : 5 frequency ratio. In contrast, symmetric velocity perturbations would lead to a uni-directional shift of the field lines in the azimuthal direction. In this case, no toroidal magnetic field component would be created, and the only allowed equilibrium solution has a vanishing δB_ϕ .

We have shown how magneto-elastic oscillations can modulate quasi-statically the magnetosphere and how the corresponding magnetic field configurations can be obtained instantaneously from the perturbations at the magnetar’s surface. The next major step towards a direct connection between the theoretical modeling and the observed QPOs in magnetar giant flares consists in taking into account an emission mechanism for which the modulations of the magnetosphere cause the observed variations of the light curve in the X-ray band. A promising candidate is resonant cyclotron scattering, as already pointed out in Gabler (2011) and Gabler et al. (2014).

ACKNOWLEDGEMENTS

Work supported by the Collaborative Research Center on Gravitational Wave Astronomy of the Deutsche Forschungsgemeinschaft (DFG SFB/Transregio 7), the Spanish *Ministerio de Educación y Ciencia* (AYA 2010-21097-C03-01), the *Generalitat Valenciana* (PROMETEO-2009-103 and PROMETEO-2011-083), and the EU through the ERC Starting Grant no. 259276-CAMAP and the ERC Advanced Grant no. 341157-COCO2CASA. Partial support comes from NewCompStar, COST Action MP1304. Computations were performed at the *Servei d’Informàtica de la Universitat de València*.

REFERENCES

- Akmal A., Pandharipande V. R., Ravenhall D. G., 1998, *Phys. Rev. C*, 58, 1804
- Beloborodov A. M., 2009, *ApJ*, 703, 1044
- Beloborodov A. M., 2013a, *ApJ*, 777, 114
- Beloborodov A. M., 2013b, *ApJ*, 762, 13
- Beloborodov A. M., Thompson C., 2007, *ApJ*, 657, 967
- Bucciantini N., Del Zanna L., 2013, *MNRAS*, 428, 71
- Cerdá-Durán P., Font J. A., Antón L., Müller E., 2008, *A&A*, 492, 937
- Cerdá-Durán P., Stergioulas N., Font J. A., 2009, *MNRAS*, 397, 1607
- Colaiuda A., Beyer H., Kokkotas K. D., 2009, *MNRAS*, 396, 1441
- Colaiuda A., Kokkotas K. D., 2011, *MNRAS*, 414, 3014

- Colaiuda A., Kokkotas K. D., 2012, MNRAS, 423, 811
- Dionysopoulou K., Alic D., Palenzuela C., Rezzolla L., Giacomazzo B., 2013, Phys. Rev. D, 88, 044020
- Douchin F., Haensel P., 2001, A&A, 380, 151
- Fernández R., Thompson C., 2007, ApJ, 660, 615
- Friedman J. L., Stergioulas N., 2013, Rotating Relativistic Stars. Cambridge University Press, Cambridge
- Gabler M., 2011, Dissertation, Technische Universität München, München
- Gabler M., Cerdá Durán P., Font J. A., Müller E., Stergioulas N., 2011, MNRAS, 410, L37
- Gabler M., Cerdá-Durán P., Font J. A., Müller E., Stergioulas N., 2013a, MNRAS, 430, 1811
- Gabler M., Cerdá-Durán P., Font J. A., Stergioulas N., Müller E., 2014, Astronomische Nachrichten, 335, 240
- Gabler M., Cerdá-Durán P., Stergioulas N., Font J. A., Müller E., 2012, MNRAS, 421, 2054
- Gabler M., Cerdá-Durán P., Stergioulas N., Font J. A., Müller E., 2013b, Physical Review Letters, 111, 211102
- Glampedakis K., Lander S. K., Andersson N., 2014, MNRAS, 437, 2
- Kojima Y., Kato Y. E., 2014, Progress of Theoretical and Experimental Physics, 2014, 020003
- Levin Y., 2007, MNRAS, 377, 159
- Link B., 2014, MNRAS, 441, 2676
- MacDonald D., Thorne K. S., 1982, MNRAS, 198, 345
- Nobili L., Turolla R., Zane S., 2008, MNRAS, 386, 1527
- Palenzuela C., 2013, MNRAS, 431, 1853
- Parfrey K., Beloborodov A. M., Hui L., 2013, ApJ, 774, 92
- Paschalidis V., Shapiro S. L., 2013, Phys. Rev. D, 88, 104031
- Passamonti A., Lander S. K., 2014, MNRAS, 438, 156
- Pavan L., Turolla R., Zane S., Nobili L., 2009, MNRAS, 395, 753
- Rea N., Zane S., Turolla R., Lyutikov M., Götz D., 2008, ApJ, 686, 1245
- Roumeliotis G., Sturrock P. A., Antiochos S. K., 1994, ApJ, 423, 847
- Sotani H., Kokkotas K. D., Stergioulas N., 2008, MNRAS, 385, L5
- Stergioulas N., Friedman J. L., 1995, ApJ, 444, 306
- Thompson C., Duncan R. C., 2001, ApJ, 561, 980
- Thompson C., Duncan R. C., Woods P. M., Kouveliotou C., Finger M. H., van Paradijs J., 2000, ApJ, 543, 340
- Thompson C., Lyutikov M., Kulkarni S. R., 2002, ApJ, 574, 332
- Timokhin A. N., Eichler D., Lyubarsky Y., 2008, ApJ, 680, 1398
- Uzdensky D. A., 2004, ApJ, 603, 652
- van Hoven M., Levin Y., 2011, MNRAS, 410, 1036
- van Hoven M., Levin Y., 2012, MNRAS, 420, 3035
- Viganò D., Pons J. A., Miralles J. A., 2011, A&A, 533, A125
- Zane S., Rea N., Turolla R., Nobili L., 2009, MNRAS, 398, 1403